International Journal of
Molecular Sciences

MDPI

Article

Fgf10 Gene Dosage from a Single Allele Is Insufficient for Forming Multilayered Epithelial Cells in the Murine Lacrimal Gland

Shiori Ikeda [1,†], Keita Sato [1,†], Yuki Tajika [2], Hirofumi Fujita [1], Tetsuya Bando [1], Tsutomu Nohno [1], Satoru Miyaishi [3] and Hideyo Ohuchi [1,*]

[1] Department of Cytology and Histology, Faculty of Medicine, Dentistry, and Pharmaceutical Sciences, Okayama University, 2-5-1 Shikata-cho, Kita-ku, Okayama 700-8558, Japan
[2] Department of Radiological Technology, Gumma Prefectural College of Health Sciences, 323-1 Kamioki-machi, Maebashi 371-0052, Japan
[3] Department of Legal Medicine, Faculty of Medicine, Dentistry, and Pharmaceutical Sciences, Okayama University, 2-5-1 Shikata-cho, Kita-ku, Okayama 700-8558, Japan
* Correspondence: ohuchi-hideyo@okayama-u.ac.jp
† These authors contributed equally to this work.

Abstract

Mutations in the fibroblast growth factor 10 (*FGF10*) gene in humans cause aplasia of the lacrimal and salivary glands (ALSG). In patients with ALSG, heterozygous loss-of-function mutations are found, and *FGF10* haploinsufficiency results in the absence of these secretory organs. Lacrimal glands (LGs) are formed through epithelial thickening, budding, and branching morphogenesis. To compare the variable phenotypes of the *Fgf10*$^{+/-}$ Harderian glands (HGs) previously reported, we examined the development of LGs in wild-type (WT), *Fgf10*$^{+/-}$, and *Fgf10*-null mice. Pax6 immunostaining was performed to visualize the LG primordia from embryonic day 15.5 (E15.5) onwards. In situ hybridization of the genes encoding the epithelial receptor of FGF10, FGFR2b, and its other ligands was performed to determine their potential involvement in LG development. LG primordia were not observed in *Fgf10*$^{+/-}$ mice bilaterally at E16.5 or later stages. At E15.5, budding from the developing conjunctival epithelium (CE) was observed in a small fraction of the *Fgf10*$^{+/-}$ LG primordia. In contrast, the *Fgf10*-null CE failed to promote budding. Among *Fgf1*, *Fgf3*, *Fgf7*, *Fgf10*, and *Fgf22*, *Fgf10* was expressed in the mesenchyme surrounding developing LG epithelial cells, whereas *Fgf1* was expressed in the LG epithelium of WT mice. *Fgf7* was initially expressed in the mesenchyme surrounding the nascent LG epithelium, but its expression subsequently became diffused. Thus, we conclude that among the FGFR2b ligands, initial LG formation is dependent on the mesenchymal factors FGF10 and FGF7, and FGF1 is likely to function as an epithelial factor in the LG primordia. A single allele of *Fgf10* was found to be insufficient to support the budding process during LG morphogenesis.

Keywords: fibroblast growth factor; *Fgf10*; *Fgf1*; *Fgf3*; *Fgf7*; *Fgf22*; *Fgfr2b*; mouse; lacrimal gland; development

Academic Editors: Sigrun Lange and Jameel M. Inal

Received: 5 February 2026
Revised: 17 February 2026
Accepted: 19 February 2026
Published: 24 February 2026

1. Introduction

The lacrimal gland (LG) contributes to the production of the aqueous portion of tears, consisting of water, electrolytes, and proteins, which protect the ocular surface of the cornea and conjunctiva. In humans, the main LG is located within the orbit of the eye, whereas in

rodents, the main LG lies exorbitally just below the auricle, with its long axis perpendicular to the zygomatic arch [1]. The exorbital LG is connected to the ocular surface by a single, long secretory duct, which then runs forward and is joined by the duct of the intraorbital LG and finally, to the lower eyelid. The developmental processes of the mouse LG and their molecular mechanisms have been well-studied [2].

Numerous factors are known to be involved in the development, cellular differentiation, tissue repair, and regeneration of the LG [2,3]. One such crucial factor is fibroblast growth factor 10 (FGF10). Since *Fgf10*-null mice lack lacrimal, Harderian, and salivary glands, *Fgf10* is required for the development of these glands [4–8]. In contrast, transgenic mouse lines in which exogenous *Fgf10* is overexpressed under a lens-specific promoter have extra glands within the cornea [5]. These results indicate that FGF10 induces LGs under competence factors such as Pax6 [4]. Thus, FGF10 is used to produce LG organoids from adult stem cells and induced pluripotent stem cells for clinical applications [9,10].

FGF10 belongs to the FGF family of extracellular secreted molecules that bind to transmembrane FGF receptors (FGFRs) for signal transduction and to extracellular matrix heparan sulfates to modulate their own functions [11]. The binding affinity of each FGF to FGFRs has been studied through a cell proliferation assay by comparison with FGF1 as the control [12,13]. FGF10 almost exclusively binds to FGFR2 isoform b (FGFR2b), although it can bind to FGFR1b with a much lower affinity. FGFR2b mRNA was found to be expressed in the developing epithelium of mouse embryos [14], whereas *Fgf10* mRNA was detected in the mesenchyme underneath or surrounding the developing epithelia, such as in limb buds, lung buds, and eyelid primordia [15–18]. Thus, FGF10–FGFR2b signaling mediates a vital mesenchymal-to-epithelial cue. As FGFs with structural similarities to FGF10 are also ligands for FGFR2b [19], the roles of FGFR2b signaling cascade in LG development have been extensively clarified [2,20,21]. Most recently, it was reported that the phospholipase C gamma (PLCγ) pathway regulates LG development, competing with phospho-inositol 3 kinase (PI3K) [22]. Intracellularly, Shp2, Sprouty 2, Kras, and Pea3 function as FGFR2b downstream effectors during mouse LG development [23–26].

The specific and indispensable involvement of FGF10 in LG development or maintenance has been deduced from a human genetic disease, aplasia of the lacrimal and salivary glands (ALSG), caused by mutations in the *FGF10* gene [27] (OMIM#180920). One allele of loss-of-function mutations in the *FGF10* gene was detected; thus, haploinsufficiency for *FGF10* underlies ALSG. However, since patients with a missense *FGF10* mutation display a different phenotype as LADD syndrome [28] (OMIM#620193), exhibiting broader anomalies with affected ears, teeth, and digits, the existence of modifier genes or a dominant negative effect of the *FGF10* mutation has been postulated as well.

As a disease model for ALSG with autosomal dominant inheritance, the phenotypes of *Fgf10*-heterozygous knockout (KO) ($Fgf10^{+/-}$) mice have been reported [18,27]. In the $Fgf10^{+/-}$ adult mouse, the LGs were absent, whereas residual salivary glands were observed, corresponding well to the clinical manifestations of ALSG patients [27]. To date, mouse $Fgf10^{+/-}$ phenotypes have been described in the LGs, salivary glands, Harderian glands (HGs), ears, lungs, tracheal submucosal glands, and craniofacial bones [29–35]. Although Puk et al. (2009) reported that a new heterozygous loss-of-function mutation in the mouse *Fgf10* gene (*Aey17*) causes atrophy of the HG [31], we recently re-examined another mouse line of $Fgf10^{+/-}$ and found that more than half of the mutant mice lost their unilateral HGs in the early postnatal period [36].

The HG was originally described as a second LG, but the products and histology of the glandular secretory unit are different: HGs exhibit tubuloalveolar glands with a wide lumen secreting lipid-rich products, whereas LGs exhibit tubuloacinar glands connected to intercalated ducts secreting serous products [3,37]. In haploinsufficient conditions,

phenotypic variability is often observed with a range of possible underlying molecular mechanisms [38]. In this study, we clarified when and how LGs deteriorated in our *Fgf10*$^{+/-}$ mouse line and compared them with HGs to obtain a phenotypic view of this disease model animal. A considerable number of *Fgf10* KO mice are available (Mouse Genome Informatics, https://www.informatics.jax.org) (MGI:1099809). Here, we describe the LG phenotype in one such strain, *Fgf10*^{tm1Ska}, where a neomycin resistance cassette replaces the exon containing the ATG [18], for the foundation of consecutive studies to elucidate the mechanisms underlying phenotypic variance in the haploinsufficiency state.

2. Results

2.1. Absence of LGs in the *Fgf10*$^{+/-}$ Mouse at 5 Weeks and Perinatal Days

In the adult *Fgf10*$^{+/-}$ mouse, adipose tissue occupies the area where the LG should normally exist [27]. The authors of that study examined two *Fgf10*$^{+/-}$ female mice at 8–9 weeks old, but whether the LG was not formed at all during development or if the once-formed LG degenerated later by the stage of sexual maturity was not clarified. In this study, we first confirmed the absence of LG in *Fgf10*$^{+/-}$ male mice at 5 weeks of age (n = 5, Figure 1, Supplementary Table S1). The LG was already replaced by adipose tissue (Figure 1D–F).

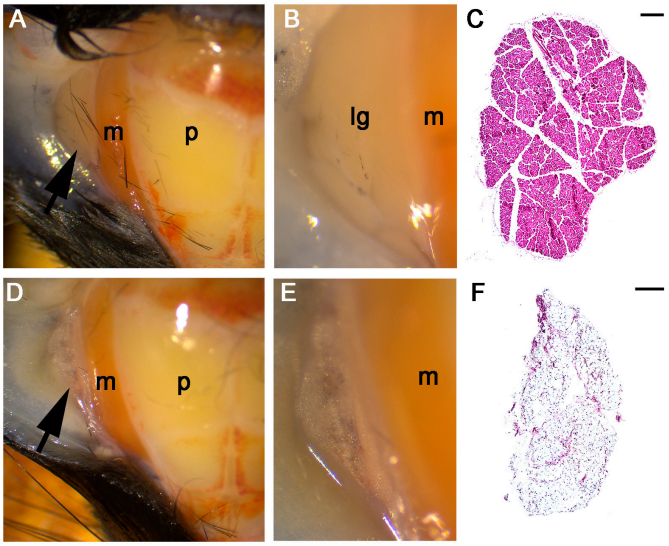

Figure 1. Absence of lacrimal glands (LGs) in the *Fgf10*$^{+/-}$ mouse. (**A**,**B**,**D**,**E**) Dorsal views of WT (**A**,**B**) and *Fgf10*$^{+/-}$ (**D**,**E**) male heads at 5 weeks, visualizing the exorbital LG (arrow in (**A**)) or that replaced by connective, fat tissue (arrow in (**D**)). Head skin was removed. LG portions (arrows in (**A**,**D**)) are enlarged in (**B**,**E**), respectively. (**C**,**F**) Histology of the WT (**C**) and *Fgf10*$^{+/-}$ degenerated (**F**) LGs at 5 weeks. m, masseter muscle; lg, lacrimal gland; p, parietal bone. Scale bars: 100 µm (in (**C**,**F**)). Photos were taken to the same scale for (**A**,**D**), (**B**,**E**), and (**C**,**F**), respectively.

As we found that the *Fgf10*$^{+/-}$ HG, a large post-bulbar gland characteristic of tetrapods, is often unilaterally degenerated by the early postnatal stage [36], we examined LG phenotypes at postnatal day 10 (P10) and earlier stages. We performed immunostaining with the anti-Pax6 antibody on P10 head sections because Pax6 identifies the LG primordia in mice [4]. None of Pax6-positive LG primordia were present in the *Fgf10*$^{+/-}$ mouse, whereas Pax6-negative developing salivary glands were observed, corresponding to submandibular, sublingual, and parotid gland primordia (Supplementary Figure S1). At P6, P0.5, and embryonic day 19 (E19), histology showed only hollow connective tissues lacking LG primordia in the *Fgf10*$^{+/-}$ mouse (Supplementary Figure S2). Whole-mount acetocarmine staining also showed the absence of LG primordia in *Fgf10*$^{+/-}$ mice at P0.5 (n = 2 for WT, n = 4 for *Fgf10*$^{+/-}$) and E19.5 (n = 2 for WT, n = 3 for *Fgf10*$^{+/-}$) (Supplementary Figure S2

and Table S1) [22]. Intraorbital LGs were also absent in *Fgf10*$^{+/-}$ mice at E19.5, as confirmed by hematoxylin–eosin (HE) staining (n = 2 for WT, n = 2 for *Fgf10*$^{+/-}$) (Supplementary Figure S3). At E18.5, we performed 3D morphological analyses on a whole head of WT or *Fgf10*$^{+/-}$ mice by correlative light microscopy and block-face imaging [39] and revealed that the LGs were absent bilaterally, while the nearby parotid glands were present in the *Fgf10*$^{+/-}$ head, as reported previously in the adult mutant [27] (Supplementary Figure S4 and Movie S1).

2.2. Absence of LGs in the *Fgf10*$^{+/-}$ Mouse in Late Embryonic Stages

We then sought to examine the embryonic LG primordia before E18.5. In developing mice, the LG emerges from ingrowing at the temporal nascent conjunctival epithelium (CE), whereas the HG develops from ingrowing at the nasal CE. Mouse LG development involves three distinct processes: thickening of the developing CE, budding from the thickened epithelium, and subsequent branching morphogenesis [2]. LG branching morphogenesis has been reported not to begin before E16 in C57BL/6J mice, being delayed compared to ICR mice [40]. Since the origin of our *Fgf10* KO mouse strain was (C57BL/6NCrlj × CBA/JNCrlj)F1 [18], we observed LG development in WT litters at E15,5, E16.5, E17, E18, and E18.5 by Pax6-immunostaining (Figure 2). At E15.5, budding from the developing CE was observed. Some sections showed isolated nascent acinar-like cells (Figure 2A), whereas other serial sections showed a bifurcation of the CE (Figure 3A) according to their horizontal levels. By E16.5, the terminal portion of the bifurcated epithelium had become multilayered and exhibited a club-like appearance (Figure 2C). At E17 and onwards, multiple isolated glandular cells were observed in the mesenchymal capsule-like sheath (Figure 2E,G,I), indicating cross-sections of branched glandular cells. In contrast, none of the *Fgf10*$^{+/-}$ embryos had Pax6-positive LG primordia from E16.5 onwards (Figure 2D,F,H,J).

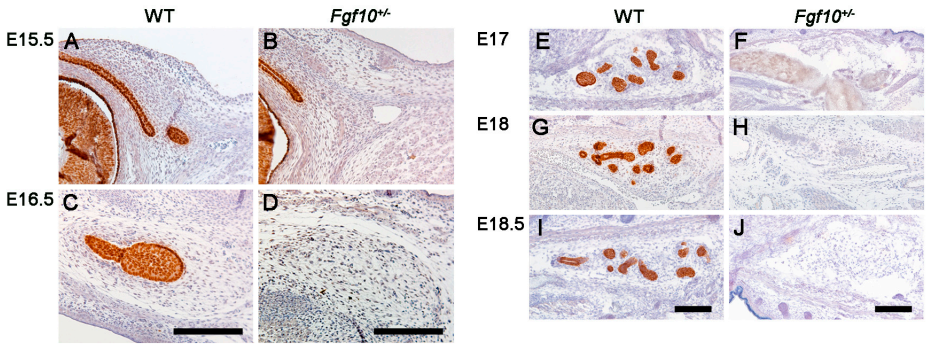

Figure 2. Pax6-immunostaining of WT (**A**,**C**,**E**,**G**,**I**) and *Fgf10*$^{+/-}$ (**B**,**D**,**F**,**H**,**J**) LG primordia at E15.5 (**A**,**B**), E16.5 (**C**,**D**), E17 (**E**,**F**), E17.5 (**G**,**H**), and E18.5 (**I**,**J**). Pax6 proteins (brown) are localized to the developing conjunctival epithelium, retina, and lacrimal glandular cells. Horizontal sections of the embryonic head are shown. The temporal side is to the right. Cell nuclei are counter-stained with hematoxylin. Scale bars: 100 μm (in (**C**,**D**,**I**,**J**)); the same scale for (**A**,**C**); (**B**,**D**); (**E**,**G**,**I**); (**F**,**H**,**J**)).

2.3. LG Primordia of the *Fgf10*$^{+/-}$ Mouse at E15.5: A Small Fraction Has Stunted Buds

In the first *Fgf10*$^{+/-}$ embryo at E15.5 examined, we could not find budding from the developing CE (Figure 2B). Since we previously found variable phenotypes in *Fgf10*$^{+/-}$ HGs, we examined multiple *Fgf10*$^{+/-}$ embryos at E15.5 and compared their phenotypes among the three genotypes. We found that most of the WT embryos at E15.5 had budding from the developing CE (n = 12 WT embryos; Figure 3A,E; Supplementary Movie S2). In contrast, three out of 22 *Fgf10*$^{+/-}$ LG primordia examined (n = 11 *Fgf10*$^{+/-}$ embryos) budded from the CE, but their subsequent growth was stunted (Figure 3B,E; Supplementary Movie S3). The remaining *Fgf10*$^{+/-}$ LG primordia had no budding, and the LG primordial

epithelium was flat or thickened only (Supplementary Movie S4), similar to that found in the *Fgf10*-null embryo (Figure 3C,E). As for *Fgf10*-null embryos, LG primordia have been shown to be absent at P0 [4]. We observed a thickened epithelium at the tip of the ingrowing CE (Figure 3D); however, none of the *Fgf10*-null embryos had budding from the CE (n = 7; Figure 3E).

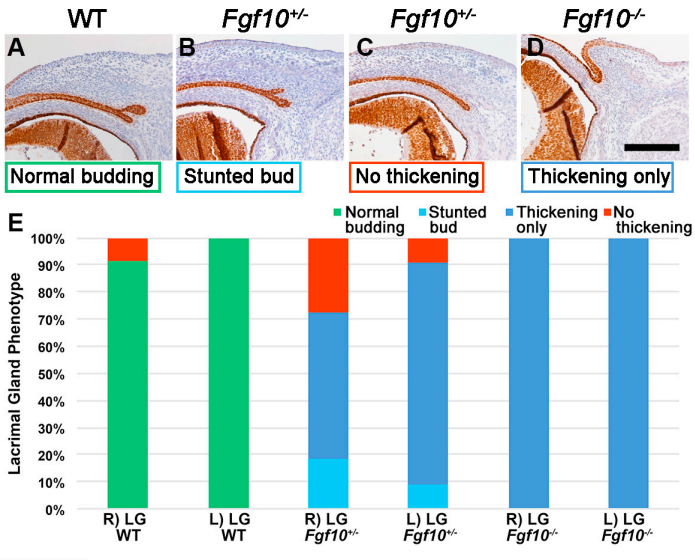

Figure 3. Pax6-immunostaining (brown) of WT (**A**), *Fgf10*$^{+/-}$ (**B**,**C**), and *Fgf10*-null (**D**) LG primordia at E15.5. Representative WT (**A**), stunted (**B**), no bud or thickening (**C**), and thickening only (**D**) LG primordia are shown. In the WT (**A**), the LG bud has a club-like appearance. The stunted bud (**B**) has a tapered appearance. Horizontal sections of the embryonic head are shown. The temporal side is to the right. Cell nuclei are counter-stained with hematoxylin. (**E**) Quantification of the LG phenotype. Pax6-immunostained histological sections of the LG primordia on both sides from WT (n = 12), *Fgf10*$^{+/-}$ (n = 11), and *Fgf10*-null (n = 7) embryos at E15.5 were observed and categorized into four groups as indicated. Scale bar: 100 μm.

2.4. Histomorphometric Analysis of HG Primordia of Fgf10$^{+/-}$ *Mice at E15.5*

As we previously reported on histology [36], Pax6-immunostaining showed that *Fgf10*$^{+/-}$ HG primordia at E15.5 had multilayered, club-like glandular cells similar to those of WT (Supplementary Figure S5A–C). To quantitatively evaluate the size of the HG primordia, we compared their length, area, and number of epithelial layers between WT and *Fgf10*$^{+/-}$ (Supplementary Figure S5E) (n = 12 for WT, n = 11 for *Fgf10*$^{+/-}$). All these parameters were significantly reduced in *Fgf10*$^{+/-}$ HGs (Supplementary Figure S5F). We also examined whether the difference in the size of the *Fgf10*$^{+/-}$ HG primordia between the right and left sides could be detected at this stage, as we found that more than half of *Fgf10*$^{+/-}$ mice exhibited unilateral HG degeneration [36]. At E15.5, none of the three parameters were significantly reduced on either side in *Fgf10*$^{+/-}$ and WT mice (Supplementary Figure S5G,H). Thus, differential developmental delay or degeneration did not occur on either side of the developing HGs at E15.5. In the *Fgf10*-null embryos, a small process for the nictitating membrane, the third eyelid, was observed, and the flanking epithelia were thickened; however, none developed multilayered, club-like glandular cells, as seen in the WT and *Fgf10*$^{+/-}$ embryos at E15.5 (n = 7, Supplementary Figure S5D).

2.5. mRNA Localization of Fgf10 and Other FGFR2b-Ligand Fgf Members During LG Development

FGF receptor type 2 isoform b (FGFR2b), whose mRNA is present in the developing epithelium [14], mediates crucial mesenchymal–epithelial signaling required for organo-

genesis, including that in the LGs [2,41]. FGFR2b ligands include FGF1, FGF3, FGF7, and FGF22, besides FGF10 [12,13], which may be synergistically involved in LG development. Therefore, we focused on these FGF members and examined their mRNA localization along with that of *Pax6* and *Fgfr2b* in WT mice. In situ hybridization (ISH) revealed that *Pax6* and *Fgfr2b* were expressed in developing LG epithelial cells at E15.5 and E18.5 (Figure 4A,A′,G,G′). As expected, distinct expression of *Fgf10* was observed in the mesenchymal cells surrounding the LG epithelial cells (Figure 4B,B′). In contrast, we found that *Fgf1* was clearly expressed in developing LG epithelial cells, similar to *Pax6* and *Fgfr2b* (Figure 4C,C′). *Fgf3* expression was not observed at E15.5 but was diffusely observed in E18.5 LG epithelial cells and the surrounding mesenchymal tissue (Figure 4D,D′). *Fgf7* was diffusely expressed in the mesenchymal tissue, but its expression was not restricted to the developing LG region (Figure 4E,E′) compared to the data obtained with sense control probes (Supplementary Figure S6). None of the *Fgf22* transcripts were detected in association with the LG primordia at E15.5 or E18.5 (Figure 4F,F′), while its mRNA was distinctly detected in developing hair follicles such as vibrissae (Supplementary Figure S7) as reported [42].

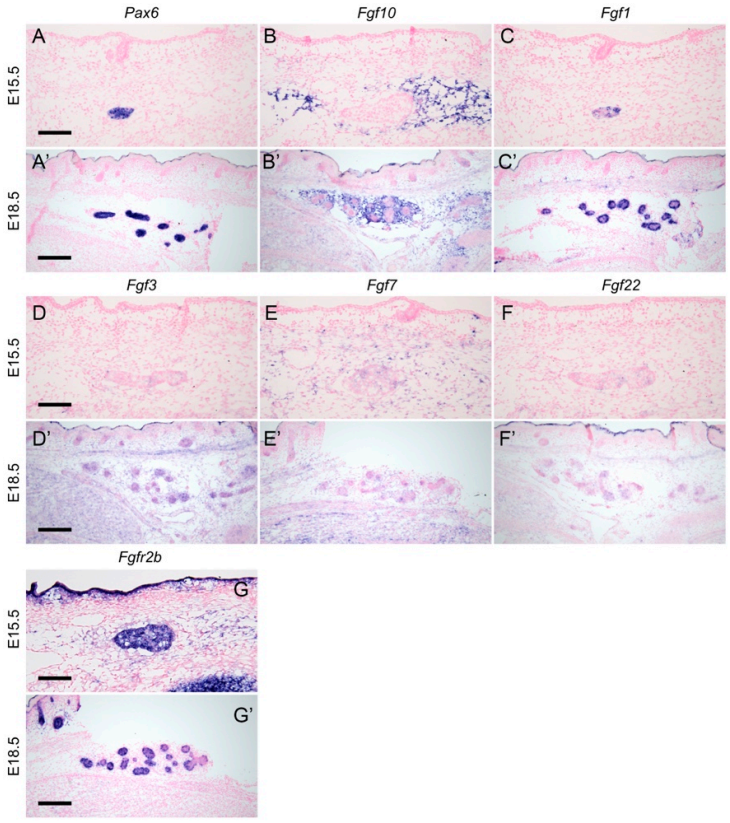

Figure 4. mRNA localization of *Fgf10* (**B**,**B′**) and other FGFR2b ligand *Fgfs* (**C**–**F**,**C′**–**F′**), along with *Pax6* (**A**,**A′**) and *Fgfr2b* (**G**,**G′**) at E15.5 and E18.5. Horizontal sections of the embryonic heads are shown. The temporal side is to the right. Cell nuclei are counter-stained with nuclear fast red. In (**E′**,**G′**), a portion of tissue was separated during sample preparation. Negative controls for each gene, hybridized with sense probes, are shown in Supplementary Figure S6. Positive internal control signals for each gene are shown in Supplementary Figure S7. Scale bars: 100 µm for E15.5; 200 µm for E18.5.

Since we found that a small fraction of *Fgf10*$^{+/-}$ LG primordia proceeded with budding from the nascent conjunctival epithelium, we examined the expression patterns of *Fgf10*, *Fgf7*, and *Fgf1* at the position of bifurcated LG primordia of *Fgf10*$^{+/-}$ mice at E15.5 (Figure 5). We found that *Fgf10* was expressed in the proximal and anterior mesenchyme of the LG bud

(Figure 5A). In contrast, *Fgf7* was expressed in the more posterior periocular mesenchyme, which was localized in the portion toward which the LG bud was elongated (Figure 5B). Two-color fluorescent ISH (FISH) verified the overlapping and differentially expressed domains of *Fgf10* and *Fgf7* (Figure 5E). As for *Fgf1*, it was expressed in both conjunctival and bifurcated LG bud epithelia (Figure 5C; compare with the sense control in Figure 5C′).

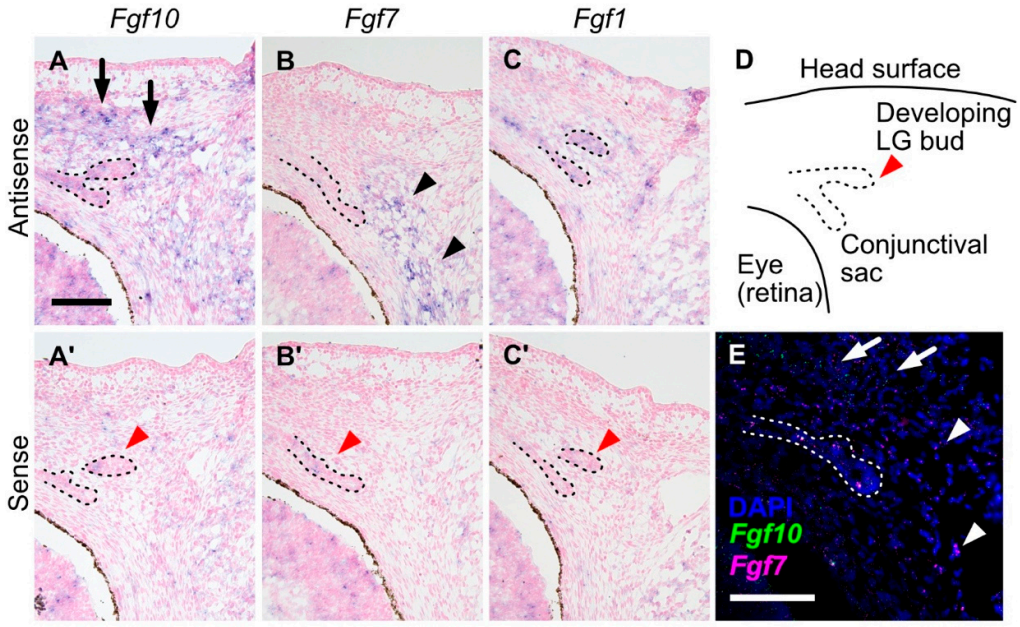

Figure 5. mRNA localization of *Fgf10*, *Fgf7*, and *Fgf1* in the bifurcating lacrimal gland primordium at E15.5. Consecutive negative control sections hybridized with sense (Se) probes are shown in (**A′**,**B′**,**C′**), respectively, where red arrowheads show the portion of the lacrimal gland bud. *Fgf10* and *Fgf7* are expressed in the periocular mesenchyme (arrows in (**A**); arrowheads in (**B**)), whereas *Fgf1* is expressed in the conjunctival and lacrimal gland epithelium (**C**). (**D**) A schematic drawing illustrates the ocular histology for (**A**–**C′**) with red arrowhead showing the lacrimal gland bud. (**E**) Two-color fluorescent in situ hybridization to visualize *Fgf10* (green) and *Fgf7* (magenta) mRNA, simultaneously. Nuclei were stained with DAPI. Arrows and arrowheads indicate regions of *Fgf10* and *Fgf7* expression. Scale bars: 100 μm.

3. Discussion

In this study, we used young male, postnatal, and embryonic mice and identified the LG phenotype in a strain of *Fgf10*$^{+/-}$ mice [18] (MGI: 1099809): *Fgf10*$^{+/-}$ LG does not develop after budding at the latest. Although Qu et al. (2011) briefly showed a similar LG phenotype in another *Fgf10*-heterozygous KO mouse [29,43], we wanted to know at what stage the *Fgf10*$^{+/-}$ LG deteriorates in the case of our strain. As Kuony et al. (2019) described [40], the developmental stage of the LG seemed to be slightly delayed in *Fgf10* KO mice with the C57BL/6J background. Pan et al. (2008) showed ectopic LG budding was induced by FGF10-soaked bead implantation into the conjunctival mesenchyme near the authentic LG bud [24]. Thus, it is tempting to reverse lacrimal gland aplasia in the *Fgf10*-heterozygous mice as a preliminary test for ALSG patients.

We visualized the WT budding portion from the developing CE wall at E15.5 on histological sections, which morphologically resembles the lateral or side branching in the mammary gland [44]. Because this budding does not occur at all in *Fgf10*-null mice, the *Fgf10* gene dosage from the two alleles is required for budding in the LG. The WT LG bud, which morphologically resembles the terminal end bud in the mammary gland, consists of a multilayered epithelium, and subsequent clefting, typically observed in the developing salivary gland, seems to advance branching morphogenesis of the LG [45]. We

witnessed the LG buds emerge in a small fraction of *Fgf10*$^{+/-}$ embryos, but the bifurcated domain exhibited merely a folding of one-cell layer cells. Thus, we suggest that the *Fgf10* gene dosage from a single allele is insufficient for forming multilayered epithelial cells to advance further branching morphogenesis. Most *Fgf10*$^{+/-}$ LG primordia (19 of 22 LGs from 11 embryos) exhibited no thickening or thickening only, implying that developmental delay [46] and phenotypic variations could obscure the definite phenotype.

Although *Fgf10*$^{+/-}$ and *Fgf10*$^{-/-}$ mice differ in the extent to which LG development proceeds, the *Fgf10* gene dosage required in the initial phase of bilateral LG development are considered rather high. This differs from the dose required for the formation of the HGs, eyelids, and limbs. Why the degree of phenotypes for these organs is so different in the *Fgf10*-heterozygous state (haploinsufficiency) is not clear, whereas all these organs are lacking in the *Fgf10*-null mouse. This is most likely due to genetic redundancy among FGFR2b ligands. It was postulated that the duration of transcriptional bursting from only one allele could not compensate for the stochastic, transiently low expression levels below the threshold required for the formation and development of organ primordia [47], which might correlate with phenotypic variations.

Organogenesis requires epithelial–mesenchymal interactions, in which FGFR2b signaling is thought to be crucial [2]. Mice and humans have 22 FGF members, and they have distinct affinities for seven types of FGF receptors [11]. FGF10 belongs to the FGF7 subfamily, which comprises FGF3, FGF22, FGF7, and FGF10. As described, FGFR2b specifically binds to the members of the FGF7 family along with FGF1 [12,13]. This study showed that *Fgf10* and *Fgf7* are expressed in the overlapping domain of mesenchyme near the developing LGs, but their expression domains are not identical. Functional redundancy with Fgf7 could partially rescue the deficiency of *Fgf10* during LG development.

We observed overlapping expression patterns of *Pax6* and *Fgfr2b* in the developing LG epithelium. Because *Fgfr2b* conditional KO mice lose *Pax6* expression in the CE [48], FGFR2 signaling is thought to be important for maintaining *Pax6* expression in ocular epithelial cells. Conversely, the transcription factor Pax6 directly regulates cell cycle exit in lens cells by binding to the *Fgfr2* gene [49]. Although these previous studies covered other ocular epithelial cell components, mutual interactions between Pax6 transcriptional control and FGFR2b signaling in the developing LG epithelium are conceivable.

Both *Pax6* and *Fgf1* are expressed in developing LG epithelial cells. FGF1 is known to bind all seven FGF receptor proteins and does not specifically activate FGFR2b [12,13]. Pan et al. (2008) reported that FGF1 binding to FGFR2b does not require heparan sulfate and that the site of the FGF1–FGFR2b binding complex is not confined to the LG bud (tip) [24]. Our ISH data also showed a rather broad expression domain of *Fgf1* in the developing conjunctival and LG epithelia, implying a unique role for FGF1 via FGFR2b and other FGFRs. FGF1 is known to maintain metabolic homeostasis and insulin sensitivity by upregulating its transcription via PPARγ gamma when exposed to a high-fat diet [50]. Therefore, it is tempting to speculate that the transcription of *Fgf1* might be likewise regulated by Pax6 in LG formation, regeneration, and homeostasis.

In the present study, we focused on male LG phenotypes in the case of adult mice to exclude the influence of sexual dimorphism on their severity because a higher prevalence in females is seen in LG disorders [51]. As in the salivary glands, sexual difference in morphology is observed in the LG of rodents and humans [52], in which acinar area in LGs of 8-week male mice is larger than female equivalents. Given that the effect of testosterone on gender-specific gene expression like lacrimal *Mup* (*Major urinary protein*) mRNA levels occur after 2 weeks [53], the influence of sex hormones on LG expansion after morphogenesis seems to begin around this stage. Therefore, after the LG morphogenesis is complete, the acinar growth is likely enhanced by sex hormones. As previously reported [27], female

Fgf10$^{+/-}$ mice also lack the LG. Although whether the precise timing of LG morphogenesis is identical between the sexes is not well determined, it is most likely that *Fgf10*$^{+/-}$ female mice also primarily fails to develop LGs as in the male.

4. Materials and Methods

4.1. Fgf10 KO Mice and Tissue Collection at Different Stages

Fgf10 KO mice used in this study have been described previously [18]. Genotyping was performed using tail DNA as previously described [36]. Male and female *Fgf10*$^{+/-}$ mice were crossed, and the morning when vaginal plugs were detected was considered day 0.5 post coitum. Embryos were collected via cesarean section at E15.5, E16.5, E17, E18, E18.5, E19, and E19.5. The numbers of embryos examined are listed in Supplementary Table S1. Postnatal (P0.5, P6, and P10) and young (5 weeks old, male) mice were processed for subsequent experimental procedures after appropriate euthanasia. Acclimatization periods for the 5-week mice to experimental locations were more than 24 h.

4.2. Fixation and Histology

The collected embryos were immediately washed in ice-cold phosphate-buffered saline (PBS), immersed in 4% paraformaldehyde (PFA)/PBS at 4 °C for 1 h, and their heads were dissected out. For P6, P10, and 5-week-old mice, transcardial perfusion fixation was performed before dissection. The heads were fixed in ice-cold 4% PFA/PBS overnight, washed with PBS, dehydrated in an ethanol series, cleared in xylene, and embedded in paraffin. Sections were cut at 5 µm, transferred onto CREST-coated glass slides (Cat. No. CRE-01; Matsunami Glass, Osaka, Japan), deparaffinized using G-NOX (GenoStaff, Tokyo, Japan), and stained with Mayer's hematoxylin (Cat. No. 1.09249.0500; Merck Millipore, Sigma-Aldrich, St. Louis, MO, USA) and Eosin Y (Cat. No. HT110116; Sigma-Aldrich) according to the standard procedure. To identify the location of the developing LGs, paraffin sections were stained with 0.05% toluidine blue (pH 7.0, Cat. no. 40981, Muto Pure Chemicals, Tokyo, Japan).

For in situ hybridization, frozen samples were prepared according to standard procedures. Cryoprotection was achieved by immersing the samples in 30% sucrose/PBS. Frozen sections were cut at 7 µm for E15.5 embryos and at 15 µm for later stages using a cryostat (Tissue-Tek Polar®; Sakura Finetek Japan, Tokyo, Japan).

4.3. Whole-Mount Acetocarmine Staining of LGs

To visualize LGs as whole mounts, acetocarmine staining was performed as previously described [22]. Briefly, fixed and trimmed mouse heads at E19.5 and P0.5 were dissected to expose the exorbital LGs and dehydrated in 70% ethanol overnight. The samples were then stained with a 0.5% carmine solution (Cat. No. C-1022; Sigma-Aldrich) prepared in 45% boiling acetic acid for 5 min. Successive destaining was performed using 70% ethanol (3 min), 1% HCl in 70% ethanol (2 min), and 5% HCl in 70% ethanol (1 min). The exorbital LGs in 70% ethanol were observed using a Leica stereomicroscope. After carmine staining, the samples were washed vigorously in 70% ethanol and processed for paraffin embedding, sectioning, deparaffinization, and HE staining to determine the presence or absence of intraorbital LGs (Supplementary Figure S3).

4.4. Correlative Microscopy and Block-Face Imaging (CoMBI)

Fixed embryonic heads (E18.5) were immersed overnight in 1% tannic acid/PBS. After cryoprotection with 30% sucrose/PBS, the samples were embedded in OCT compound and sectioned at 15 µm with a cryostat. Three-dimensional imaging using CoMBI was performed as previously described [39,54]. Briefly, the block-faces were captured serially

using a digital camera (Sony α7RIII, Tokyo, Japan) with a macro lens (Tamron SP AF 180 mm F/3.5 Di LD [IF] MACRO 1:1 (Model B01), Saitama, Japan) and a teleconverter (Kenko Digital Teleplus Pro 300 2× DGX, Tokyo, Japan). Segmentation of the LGs and parotid glands was performed manually. As landmarks, the eyeball, lens, optic nerve, mandibular ramus, and inner ear were manually segmented and reconstructed using a 3D slicer (https://www.slicer.org). To verify the interpretation of the structures in the block-face images, several sections were stained with 0.05% toluidine blue, and their histology was correlated with the block-face images, as shown in Supplementary Figure S4.

4.5. Immunohistochemistry

Immunohistochemistry was performed on deparaffinized sections according to standard procedures. Briefly, the sections were antigen-retrieved, immersed in 10 mM citrate buffer (pH 6.0), and heat-treated in a pressure cooker (124 °C, 10 min). After sections were cooled to room temperature, they were washed with H_2O and quenched against endogenous peroxidase using BLOXALL (Cat. No. SP-6000; Vector Laboratories, Newark, CA, USA) for 10 min, washed in PBS-Tween 20 (0.05%), and blocked with 2.5% normal horse serum (NHS). Next, anti-Pax6 antibody (rabbit, diluted 1:2000 in 2.5% NHS, Cat. No. 901301; BioLegend, San Diego, CA, USA) was added to the sections and incubated at room temperature for 1 h. After washing, ImmPRESS Peroxidase Polymer anti-rabbit IgG reagent (Cat. No. MP-7401; Vector Laboratories) was added, incubated for 10 min, washed with PBS-Tween, and visualized by incubation with the ImmPACT DAB EqV substrate (Cat. No. SK-4103; Vector Laboratories) for 2 min. After vigorous washing in H_2O and PBS, and 1 min counterstaining with Mayer's hematoxylin, the sections were mounted with a mixture of polyvinyl alcohol/glycerol. For frozen sections, antigen retrieval was shortened to 5 min at 95 °C in a thermo pot for better preservation of sections.

4.6. ISH

Conventional ISH was performed as previously described [36,55]. Target cDNAs were amplified from mouse brain first-strand cDNA by PCR using the primers listed in Supplementary Table S2 and inserted into the pBluescript II KS(+) vector. To generate digoxigenin-labeled riboprobes, template cDNAs flanked with T3, T7, and/or SP6 RNA promoters were prepared by PCR. For *Fgf22*, *Fgfr2b*, and *Pax6*, the coding regions were used as probes. For *Fgf10*, *Fgf7*, *Fgf1*, and *Fgf3*, 5′-untranslated regions were included in addition to the coding regions for the probes. The 3′-untranslated regions were not included in probe sequences not to detect signals when hybridized with sense probes. Two-color FISH was performed using signal amplification by exchange reaction (SABER)-FISH combined with hybridization chain reaction (HCR) according to previous reports [56,57]. HCR hairpins were prepared according to a previous report [58] Briefly, DNA hairpins labeled at the 5′ end with a C12-amino linker (IDT, Coralville, IA, USA) dissolved in 0.1 M sodium borate buffer (pH 8.5) was mixed with the N-hydroxysuccinimide esters of ATTO488 for S9_H1 and S9_H2 and with ATTO565 for S25_H1 and S25 H2 dissolved in dimethylformamide for coupling reaction. Fluorophore-conjugated DNAs were purified by denaturing polyacrylamide gel electrophoresis with 20% polyacrylamide gels. The DNA oligos used in SABER-HCR-FISH and related information are listed in Supplementary Table S3.

4.7. Image Capture and Processing

For dissection and observation of the dissected samples, a Leica dissecting microscope (M165FC or S9D; Leica Microsystems, Wetzlar, Germany) equipped with a digital camera was used (DFC310 FX or FLEXACAM C1; Leica Microsystems). Sections were observed under a Leica microscope (DM5000B; Leica Microsystems) or a Carl Zeiss Axioplan microscope (Carl Zeiss, Oberkochen, Germany). Images were captured using a digital camera

(DS-Fi1; Nikon, Tokyo, Japan) or an IDS UI-3290SE-C-HQ camera (Imaging Development Systems, Obersulm, Germany). To identify the horizontal level of the sections, images were captured using a Keyence microscope with a 4x objective lens (BZ-X700; Keyence, Osaka, Japan) (CRL_552; Core Facility Portal, Okayama University). Fluorescence images were acquired using an IX71 inverted microscope (Olympus, Tokyo, Japan) equipped with an sCMOS camera (pco.panda 4.2; Excelitas PCO GmbH, Kelheim, Germany).

4.8. Histomorphometric Analysis and Statistics

Pax6 immunostaining was performed on 10–24 horizontal sections per individual embryonic head at E15.5 (n = 12 for WT, n = 11 for *Fgf10*$^{+/-}$, and n = 7 for *Fgf10*$^{-/-}$), and sections containing the largest HGs were selected and digitally photographed. The length, area, and number of epithelial layers were measured from the images as shown in Supplementary Figure S5. The average values were tested for significance using Student's t-test. The graph was drawn as an Excel scatter plot, and the error bars indicate the standard deviation (SD). The same Pax6-immunostained sections were examined for the LG phenotype and categorized into four morphologically distinct types: normal budding, stunted buds, thickening only, and no thickening (Figure 3).

Supplementary Materials: The following supporting information can be downloaded at https://www.mdpi.com/article/10.3390/ijms27052113/s1.

Author Contributions: Conceptualization, S.I. and H.O.; methodology, S.I., K.S., Y.T. and H.O.; software, S.I., K.S., Y.T. and H.O.; validation, S.I., K.S., Y.T. and H.O.; formal analysis, S.I., K.S., Y.T. and H.O.; investigation, S.I., K.S. and Y.T.; resources, K.S., Y.T., S.M. and H.O.; data curation, S.I., K.S., Y.T. and H.O.; writing—original draft preparation, K.S. and H.O.; writing—review and editing, S.I., K.S., Y.T., H.F., T.B., T.N., S.M. and H.O.; visualization, S.I., K.S., Y.T. and H.O.; supervision, K.S., T.N. and H.O.; project administration, K.S. and H.O.; funding acquisition, S.I., K.S. and H.O. All authors have read and agreed to the published version of the manuscript.

Funding: This work was supported by JSPS KAKENHI Grant Number JP25H00312, JP24K09998, JP23K05850, JP24K21962, Frontier Photonic Sciences Project of National Institutes of Natural Sciences (Grant Number 01212503), and research grants from the Japan Health Foundation and the Japan Foundation for Applied Enzymology.

Institutional Review Board Statement: The animal study protocol was approved by the Institutional Review Board of Okayama University (protocol code: OKU-2023243 and OKU-2025598, dated 1 April 2023 and 27 August 2025, respectively).

Informed Consent Statement: Not applicable.

Data Availability Statement: The original contributions presented in this study are included in the article/Supplementary Materials. Further inquiries can be directed to the corresponding author.

Acknowledgments: We thank Central Research Laboratory, Okayama University Medical School for support in preparing histological specimens.

Conflicts of Interest: The authors declare no conflicts of interest. The funders had no role in the design of the study; in the collection, analyses, or interpretation of data; in the writing of the manuscript; or in the decision to publish the results.

Abbreviations

ALSG	aplasia of lacrimal and salivary glands
C57BL/6	C57 black 6
CE	conjunctival epithelium
CoMBI	correlative microscopy and block-face imaging

DAPI	4′,6-diamidino-2-phenylindole
DNA	deoxynucleic acid
E15.5	embryonic day 15.5
FGF10, Fgf10	fibroblast growth factor 10
FGFR2b, Fgfr2b	fibroblast growth factor receptor 2, isoform b
HCR	hybridization chain reaction
HE	Hematoxylin and Eosin
HG	Harderian gland
ICR	institute of cancer research
ISH	in situ hybridization
KO	Knockout
LG	lacrimal gland
NHS	normal horse serum
OCT	optimal cutting temperature
P10	postnatal day 10
Pax6	paired homeobox gene 6
PER	primer exchange reaction
PBS	phosphate-buffered saline
PFA	Paraformaldehyde
SABER-FISH	signal amplification by exchange reaction-fluorescence ISH
WT	wild-type

References

1. Dartt, D.A. Neural regulation of lacrimal gland secretory processes: Relevance in dry eye diseases. *Prog. Retin. Eye Res.* **2009**, *28*, 155–177. [CrossRef]
2. Garg, A.; Zhang, X. Lacrimal gland development: From signaling interactions to regenerative medicine. *Dev. Dyn.* **2017**, *246*, 970–980. [CrossRef] [PubMed]
3. Khan, S.; Fitch, S.; Knox, S.; Arora, R. Exocrine gland structure-function relationships. *Development* **2022**, *149*, dev197657. [CrossRef] [PubMed]
4. Makarenkova, H.P.; Ito, M.; Govindarajan, V.; Faber, S.C.; Sun, L.; McMahon, G.; Overbeek, P.A.; Lang, R.A. FGF10 is an inducer and Pax6 a competence factor for lacrimal gland development. *Development* **2000**, *127*, 2563–2572. [CrossRef] [PubMed]
5. Govindarajan, V.; Ito, M.; Makarenkova, H.P.; Lang, R.A.; Overbeek, P.A. Endogenous and ectopic gland induction by FGF-10. *Dev. Biol.* **2000**, *225*, 188–200. [CrossRef]
6. Ohuchi, H.; Hori, Y.; Yamasaki, M.; Harada, H.; Sekine, K.; Kato, S.; Itoh, N. FGF10 acts as a major ligand for FGF receptor 2 IIIb in mouse multi-organ development. *Biochem. Biophys. Res. Commun.* **2000**, *277*, 643–649. [CrossRef]
7. Jaskoll, T.; Abichaker, G.; Witcher, D.; Sala, F.G.; Bellusci, S.; Hajihosseini, M.K.; Melnick, M. FGF10/FGFR2b signaling plays essential roles during in vivo embryonic submandibular salivary gland morphogenesis. *BMC Dev. Biol.* **2005**, *5*, 11. [CrossRef]
8. Steinberg, Z.; Myers, C.; Heim, V.M.; Lathrop, C.A.; Rebustini, I.T.; Stewart, J.S.; Larsen, M.; Hoffman, M.P. FGFR2b signaling regulates ex vivo submandibular gland epithelial cell proliferation and branching morphogenesis. *Development* **2005**, *132*, 1223–1234. [CrossRef]
9. Bannier-Helaouet, M.; Post, Y.; Korving, J.; Trani Bustos, M.; Gehart, H.; Begthel, H.; Bar-Ephraim, Y.E.; van der Vaart, J.; Kalmann, R.; Imhoff, S.M.; et al. Exploring the human lacrimal gland using organoids and single-cell sequencing. *Cell Stem Cell* **2021**, *28*, 1221–1232.e7. [CrossRef]
10. Hayashi, R.; Okubo, T.; Kudo, Y.; Ishikawa, Y.; Imaizumi, T.; Suzuki, K.; Shibata, S.; Katayama, T.; Park, S.J.; Young, R.D.; et al. Generation of 3D lacrimal gland organoids from human pluripotent stem cells. *Nature* **2022**, *605*, 126–131. [CrossRef]
11. Ornitz, D.M.; Itoh, N. New developments in the biology of fibroblast growth factors. *WIREs Mech. Dis.* **2022**, *14*, e1549. [CrossRef] [PubMed]
12. Ornitz, D.M.; Xu, J.; Colvin, J.S.; McEwen, D.G.; MacArthur, C.A.; Coulier, F.; Gao, G.; Goldfarb, M. Receptor specificity of the fibroblast growth factor family. *J. Biol. Chem.* **1996**, *271*, 15292–15297. [CrossRef] [PubMed]
13. Zhang, X.; Ibrahimi, O.A.; Olsen, S.K.; Umemori, H.; Mohammadi, M.; Ornitz, D.M. Receptor specificity of the fibroblast growth factor family. The complete mammalian FGF family. *J. Biol. Chem.* **2006**, *281*, 15694–15700. [CrossRef] [PubMed]
14. Orr-Urtreger, A.; Bedford, M.T.; Burakova, T.; Arman, E.; Zimmer, Y.; Yayon, A.; Givol, D.; Lonai, P. Developmental localization of the splicing alternatives of fibroblast growth factor receptor-2 (FGFR2). *Dev. Biol.* **1993**, *158*, 475–486. [CrossRef]

15. Yamasaki, M.; Miyake, A.; Tagashira, S.; Itoh, N. Structure and expression of the rat mRNA encoding a novel member of the fibroblast growth factor family. *J. Biol. Chem.* **1996**, *271*, 15918–15921. [CrossRef]
16. Ohuchi, H.; Nakagawa, T.; Yamamoto, A.; Araga, A.; Ohata, T.; Ishimaru, Y.; Yoshioka, H.; Kuwana, T.; Nohno, T.; Yamasaki, M.; et al. The mesenchymal factor, FGF10, initiates and maintains the outgrowth of the chick limb bud through interaction with FGF8, an apical ectodermal factor. *Development* **1997**, *124*, 2235–2244. [CrossRef]
17. Bellusci, S.; Grindley, J.; Emoto, H.; Itoh, N.; Hogan, B.L. Fibroblast growth factor 10 (FGF10) and branching morphogenesis in the embryonic mouse lung. *Development* **1997**, *124*, 4867–4878. [CrossRef]
18. Sekine, K.; Ohuchi, H.; Fujiwara, M.; Yamasaki, M.; Yoshizawa, T.; Sato, T.; Yagishita, N.; Matsui, D.; Koga, Y.; Itoh, N.; et al. Fgf10 is essential for limb and lung formation. *Nat. Genet.* **1999**, *21*, 138–141, Correction in *Nat. Genet.* **2019**, *51*, 921. https://doi.org/10.1038/s41588-019-0396-9. [CrossRef]
19. Zinkle, A.; Mohammadi, M. Structural Biology of the FGF7 Subfamily. *Front. Genet.* **2019**, *10*, 102. [CrossRef]
20. Lovicu, F.J.; Kao, W.W.; Overbeek, P.A. Ectopic gland induction by lens-specific expression of keratinocyte growth factor (FGF-7) in transgenic mice. *Mech. Dev.* **1999**, *88*, 43–53. [CrossRef]
21. Makarenkova, H.P.; Hoffman, M.P.; Beenken, A.; Eliseenkova, A.V.; Meech, R.; Tsau, C.; Patel, V.N.; Lang, R.A.; Mohammadi, M. Differential interactions of FGFs with heparan sulfate control gradient formation and branching morphogenesis. *Sci. Signal.* **2009**, *2*, ra55. [CrossRef] [PubMed]
22. Wang, Q.; Tao, C.; Wu, Y.; Anderson, K.E.; Makrides, N.; Hannan, A.; Peregrin, J.; Lin, C.S.; Ding, Z.; Li, W.; et al. FGF-induced phospholipase Cγ signaling regulates lacrimal gland branching by competing with PI3K in phosphoinositide metabolism. *Cell Rep.* **2025**, *44*, 116046. [CrossRef] [PubMed]
23. Pan, Y.; Carbe, C.; Powers, A.; Feng, G.S.; Zhang, X. Sprouty2-modulated Kras signaling rescues Shp2 deficiency during lens and lacrimal gland development. *Development* **2010**, *137*, 1085–1093. [CrossRef] [PubMed]
24. Pan, Y.; Carbe, C.; Powers, A.; Zhang, E.E.; Esko, J.D.; Grobe, K.; Feng, G.S.; Zhang, X. Bud specific N-sulfation of heparan sulfate regulates Shp2-dependent FGF signaling during lacrimal gland induction. *Development* **2008**, *135*, 301–310. [CrossRef]
25. Wang, Q.; Tao, C.; Hannan, A.; Yoon, S.; Min, X.; Peregrin, J.; Qu, X.; Li, H.; Yu, H.; Zhao, J.; et al. Lacrimal gland budding requires PI3K-dependent suppression of EGF signaling. *Sci. Adv.* **2021**, *7*, eabf1068. [CrossRef]
26. Garg, A.; Hannan, A.; Wang, Q.; Collins, T.; Teng, S.; Bansal, M.; Zhong, J.; Xu, K.; Zhang, X. FGF-induced Pea3 transcription factors program the genetic landscape for cell fate determination. *PLoS Genet.* **2018**, *14*, e1007660. [CrossRef]
27. Entesarian, M.; Matsson, H.; Klar, J.; Bergendal, B.; Olson, L.; Arakaki, R.; Hayashi, Y.; Ohuchi, H.; Falahat, B.; Bolstad, A.I.; et al. Mutations in the gene encoding fibroblast growth factor 10 are associated with aplasia of lacrimal and salivary glands. *Nat. Genet.* **2005**, *37*, 125–127. [CrossRef]
28. Rohmann, E.; Brunner, H.G.; Kayserili, H.; Uyguner, O.; Nurnberg, G.; Lew, E.D.; Dobbie, A.; Eswarakumar, V.P.; Uzumcu, A.; Ulubil-Emeroglu, M.; et al. Mutations in different components of FGF signaling in LADD syndrome. *Nat. Genet.* **2006**, *38*, 414–417, Erratum in *Nat. Genet.* **2006**, *38*, 495. [CrossRef]
29. Qu, X.; Carbe, C.; Tao, C.; Powers, A.; Lawrence, R.; van Kuppevelt, T.H.; Cardoso, W.V.; Grobe, K.; Esko, J.D.; Zhang, X. Lacrimal gland development and Fgf10-Fgfr2b signaling are controlled by 2-O- and 6-O-sulfated heparan sulfate. *J. Biol. Chem.* **2011**, *286*, 14435–14444. [CrossRef]
30. May, A.J.; Chatzeli, L.; Proctor, G.B.; Tucker, A.S. Salivary Gland Dysplasia in Fgf10 Heterozygous Mice: A New Mouse Model of Xerostomia. *Curr. Mol. Med.* **2015**, *15*, 674–682. [CrossRef]
31. Puk, O.; Esposito, I.; Soker, T.; Loster, J.; Budde, B.; Nurnberg, P.; Michel-Soewarto, D.; Fuchs, H.; Wolf, E.; Hrabe de Angelis, M.; et al. A new Fgf10 mutation in the mouse leads to atrophy of the harderian gland and slit-eye phenotype in heterozygotes: A novel model for dry-eye disease? *Investig. Ophthalmol. Vis. Sci.* **2009**, *50*, 4311–4318. [CrossRef]
32. Urness, L.D.; Wang, X.; Shibata, S.; Ohyama, T.; Mansour, S.L. Fgf10 is required for specification of non-sensory regions of the cochlear epithelium. *Dev. Biol.* **2015**, *400*, 59–71. [CrossRef]
33. Chao, C.M.; Yahya, F.; Moiseenko, A.; Tiozzo, C.; Shrestha, A.; Ahmadvand, N.; El Agha, E.; Quantius, J.; Dilai, S.; Kheirollahi, V.; et al. Fgf10 deficiency is causative for lethality in a mouse model of bronchopulmonary dysplasia. *J. Pathol.* **2017**, *241*, 91–103. [CrossRef] [PubMed]
34. May, A.J.; Teshima, T.H.N.; Noble, A.; Tucker, A.S. FGF10 is an essential regulator of tracheal submucosal gland morphogenesis. *Dev. Biol.* **2019**, *451*, 158–166. [CrossRef] [PubMed]
35. Tan, J.; Jones, M.L.M.; Teague, W.J.; Ranjitkar, S.; Anderson, P.J. Craniofacial anomalies in a murine model of heterozygous fibroblast growth factor 10 gene mutation. *Orthod. Craniofac. Res.* **2024**, *27*, 84–94. [CrossRef] [PubMed]
36. Ikeda, S.; Sato, K.; Fujita, H.; Ono-Minagi, H.; Miyaishi, S.; Nohno, T.; Ohuchi, H. Harderian Gland Development and Degeneration in the Fgf10-Deficient Heterozygous Mouse. *J. Dev. Biol.* **2024**, *12*, 16. [CrossRef]
37. Sakai, T. The mammalian Harderian gland: Morphology, biochemistry, function and phylogeny. *Arch. Histol. Jpn.* **1981**, *44*, 299–333. [CrossRef]

38. Veitia, R.A.; Birchler, J.A. Dominance and gene dosage balance in health and disease: Why levels matter! *J. Pathol.* **2010**, *220*, 174–185. [CrossRef]
39. Tajika, Y.; Murakami, T.; Iijima, K.; Gotoh, H.; Takahashi-Ikezawa, M.; Ueno, H.; Yoshimoto, Y.; Yorifuji, H. A novel imaging method for correlating 2D light microscopic data and 3D volume data based on block-face imaging. *Sci. Rep.* **2017**, *7*, 3645. [CrossRef]
40. Kuony, A.; Ikkala, K.; Kalha, S.; Magalhaes, A.C.; Pirttiniemi, A.; Michon, F. Ectodysplasin-A signaling is a key integrator in the lacrimal gland-cornea feedback loop. *Development* **2019**, *146*, dev176693. [CrossRef]
41. De Moerlooze, L.; Spencer-Dene, B.; Revest, J.M.; Hajihosseini, M.; Rosewell, I.; Dickson, C. An important role for the IIIb isoform of fibroblast growth factor receptor 2 (FGFR2) in mesenchymal-epithelial signalling during mouse organogenesis. *Development* **2000**, *127*, 483–492. [CrossRef]
42. Nakatake, Y.; Hoshikawa, M.; Asaki, T.; Kassai, Y.; Itoh, N. Identification of a novel fibroblast growth factor, FGF-22, preferentially expressed in the inner root sheath of the hair follicle. *Biochim. Biophys. Acta* **2001**, *1517*, 460–463. [CrossRef]
43. Min, H.; Danilenko, D.M.; Scully, S.A.; Bolon, B.; Ring, B.D.; Tarpley, J.E.; DeRose, M.; Simonet, W.S. Fgf-10 is required for both limb and lung development and exhibits striking functional similarity to Drosophila branchless. *Genes. Dev.* **1998**, *12*, 3156–3161. [CrossRef] [PubMed]
44. Myllymaki, S.M.; Mikkola, M.L. Inductive signals in branching morphogenesis—Lessons from mammary and salivary glands. *Curr. Opin. Cell Biol.* **2019**, *61*, 72–78. [CrossRef] [PubMed]
45. Goodwin, K.; Nelson, C.M. Branching morphogenesis. *Development* **2020**, *147*, dev184499. [CrossRef] [PubMed]
46. Geyer, S.H.; Reissig, L.; Rose, J.; Wilson, R.; Prin, F.; Szumska, D.; Ramirez-Solis, R.; Tudor, C.; White, J.; Mohun, T.J.; et al. A staging system for correct phenotype interpretation of mouse embryos harvested on embryonic day 14 (E14.5). *J. Anat.* **2017**, *230*, 710–719. [CrossRef]
47. Cook, D.L.; Gerber, A.N.; Tapscott, S.J. Modeling stochastic gene expression: Implications for haploinsufficiency. *Proc. Natl. Acad. Sci. USA* **1998**, *95*, 15641–15646. [CrossRef]
48. Zhang, J.; Upadhya, D.; Lu, L.; Reneker, L.W. Fibroblast growth factor receptor 2 (FGFR2) is required for corneal epithelial cell proliferation and differentiation during embryonic development. *PLoS ONE* **2015**, *10*, e0117089. [CrossRef]
49. Sun, J.; Rockowitz, S.; Xie, Q.; Ashery-Padan, R.; Zheng, D.; Cvekl, A. Identification of in vivo DNA-binding mechanisms of Pax6 and reconstruction of Pax6-dependent gene regulatory networks during forebrain and lens development. *Nucleic Acids Res.* **2015**, *43*, 6827–6846. [CrossRef]
50. Jonker, J.W.; Suh, J.M.; Atkins, A.R.; Ahmadian, M.; Li, P.; Whyte, J.; He, M.; Juguilon, H.; Yin, Y.Q.; Phillips, C.T.; et al. A PPARgamma-FGF1 axis is required for adaptive adipose remodelling and metabolic homeostasis. *Nature* **2012**, *485*, 391–394. [CrossRef]
51. Kastelan, S.; Hat, K.; Tomic, Z.; Matejic, T.; Gotovac, N. Sex Differences in the Lacrimal Gland: Implications for Dry Eye Disease. *Int. J. Mol. Sci.* **2025**, *26*, 3833. [CrossRef] [PubMed]
52. Cornell-Bell, A.H.; Sullivan, D.A.; Allansmith, M.R. Gender-related differences in the morphology of the lacrimal gland. *Investig. Ophthalmol. Vis. Sci.* **1985**, *26*, 1170–1175. [PubMed]
53. Shaw, P.H.; Held, W.A.; Hastie, N.D. The gene family for major urinary proteins: Expression in several secretory tissues of the mouse. *Cell* **1983**, *32*, 755–761. [CrossRef] [PubMed]
54. Tajika, Y.; Ishii, N.; Morimura, Y.; Fukuda, K.; Shikada, M.; Murakami, T.; Ichinose, S.; Yoshimoto, Y.; Iwasaki, H. Correlative microscopy and block-face imaging (CoMBI): A 3D imaging method with wide applicability in the field of biological science. *Anat. Sci. Int.* **2023**, *98*, 353–359. [CrossRef]
55. Sato, K.; Yamashita, T.; Ohuchi, H. Mammalian type opsin 5 preferentially activates G14 in Gq-type G proteins triggering intracellular calcium response. *J. Biol. Chem.* **2023**, *299*, 105020. [CrossRef]
56. Kishi, J.Y.; Lapan, S.W.; Beliveau, B.J.; West, E.R.; Zhu, A.; Sasaki, H.M.; Saka, S.K.; Wang, Y.; Cepko, C.L.; Yin, P. SABER amplifies FISH: Enhanced multiplexed imaging of RNA and DNA in cells and tissues. *Nat. Methods* **2019**, *16*, 533–544. [CrossRef]
57. Ustyantsev, K.; Stranges, M.; Volpe, F.G.; de Boer, J.F.; Kuipers, F.; Mouton, S.; Berezikov, E. One probe fits all: A highly customizable modular RNA in situ hybridization platform expanding the application of SABER DNA probes. *Development* **2025**, *152*, dev204775. [CrossRef]
58. Tsuneoka, Y.; Funato, H. Modified in situ Hybridization Chain Reaction Using Short Hairpin DNAs. *Front. Mol. Neurosci.* **2020**, *13*, 75. [CrossRef]